FINAL REPORT

submitted to

National Aeronautics and Space Administration
Lyndon B. Johnson Space Center
Space Science Branch, Code SN3
ATTN: Eric L. Christiansen
Houston, TX 77058

for research entitled

COUPLING OF SPH AND FINITE ELEMENT CODES FOR MULTI-LAYER ORBITAL DEBRIS SHIELD DESIGN

(NAG9-808)

Submitted by

Eric P. Fahrenthold
Department of Mechanical Engineering
University of Texas
Austin, TX 78712

August 8, 1997

ABSTRACT

Particle-based hydrodynamics models offer distinct advantages over Eulerian and Lagrangian hydrocodes in particular shock physics applications. Particle models are designed to avoid the mesh distortion and state variable diffusion problems which can hinder the effective use of Lagrangian and Eulerian codes respectively. However conventional particle-in-cell and smooth particle hydrodynamics methods employ particles which are actually moving interpolation points. A new particle-based modeling methodology, termed Hamiltonian particle hydrodynamics, was developed by Fahrenthold and Koo (1997) to provide an alternative, fully Lagrangian, energy-based approach to shock physics simulations. This alternative formulation avoids the tensile and boundary instabilities associated with standard smooth particle hydrodynamics formulations and the diffusive grid-to-particle mapping schemes characteristic of particle-in-cell methods.

In the work described herein, the method of Fahrenthold and Koo (1997) has been extended, by coupling the aforementioned hydrodynamic particle model to a hexahedral finite element based description of the continuum dynamics. The resulting continuum model retains all of the features (including general contact-impact effects) of Hamiltonian particle hydrodynamics, while in addition accounting for tensile strength, plasticity, and damage effects important in the simulation of hypervelocity impact on orbital debris shielding. A three dimensional, vectorized, and autotasked implementation of the extended particle method described here has been coded for application to orbital debris shielding design. Source code for the pre-processor (PREP), analysis code (EXOS), post-processor (POST), and rezoner (ZONE), have been delivered separately, along with a User's Guide describing installation and application of the software.

ACKNOWLEDGMENTS

This work was funded through the Space Science Branch of NASA Johnson Space Center under the NASA Regional Universities Grant Program. The assistance of Eric L. Christiansen (NASA Technical Officer), Jeanne L. Crews, and Justin H. Kerr of the Space Science Branch of Johnson Space Center has been greatly appreciated.

The color graphics shown in Appendices A, B, and C were produced by Philip Watson of the Visualization Lab at the University of Texas at Austin.

TABLE OF CONTENTS

1. Introduction

The Hamiltonian particle dynamics model developed by Fahrenthold and Koo (1997) is purely hydrodynamic. In order to account for strength effects important in the simulation of hypervelocity impacts on space structures, the aforementioned model has been extended, to incorporate elastic-plastic-damage effects. These effects are quantified using a three dimensional, hexahedral finite element characterization of deformation in the modeled continuum.

The extension of the particle model of Fahrenthold and Koo (1997), described here, is based on a body centered cubic packing scheme for the material particles. Under such a packing scheme, each particle has eight nearest neighbors in the reference configuration. The center of mass coordinates of these eight nearest neighbors are designated as nodal coordinates for a hexahedral finite element centered initially on the particle. The volume of this element is calculated at each time step (using one point integration), and appears as a mechanical variable in the system level internal energy function. The relative velocity of the body centered particle, with respect to each of its nearest neighbors, is calculated at each time step to determine the local plastic strain rate. Finally a scalar continuum damage variable is introduced for each element, allowing for the loss of cohesion of the element when a user-specified level of plastic strain has been accumulated.

The sections which follow describe in detail the hexahedral finite element based elastic-plastic-damage model implemented in the code EXOS, and illustrate application of the code by the simulation of example hypervelocity impact problems. A User's Guide for the analysis code EXOS, pre-processor PREP, post-processor POST, and rezoner ZONE is provided separately. In the interest of brevity the current report describes only the new finite element based augmentations developed to extend the model of Fahrenthold and Koo(1997). The reader is referred to the latter reference for a detailed description of the basic Hamiltonian particle hydrodynamics model.

2. Kinematics

The hexahedral element kinematics are similar to those employed in Lagrangian hydrocodes, for example DYNA3D (Hallquist, 1983). The components of the deformation gradient ($f_{jk}^{(i)}$) for element 'i' are calculated as

$$f_{11}^{(i)} = [\, c_1^{(i,2)} - c_1^{(i,1)} + c_1^{(i,3)} - c_1^{(i,4)} + c_1^{(i,6)} - c_1^{(i,5)} + c_1^{(i,7)} - c_1^{(i,8)} \,] / 8 \qquad (1a)$$

$$f_{21}^{(i)} = [\, c_2^{(i,2)} - c_2^{(i,1)} + c_2^{(i,3)} - c_2^{(i,4)} + c_2^{(i,6)} - c_2^{(i,5)} + c_2^{(i,7)} - c_2^{(i,8)} \,] / 8 \qquad (1b)$$

$$f_{31}^{(i)} = [\, c_3^{(i,2)} - c_3^{(i,1)} + c_3^{(i,3)} - c_3^{(i,4)} + c_3^{(i,6)} - c_3^{(i,5)} + c_3^{(i,7)} - c_3^{(i,8)} \,] / 8 \qquad (1c)$$

$$f_{12}^{(i)} = [\, c_1^{(i,3)} - c_1^{(i,2)} + c_1^{(i,4)} - c_1^{(i,1)} + c_1^{(i,7)} - c_1^{(i,6)} + c_1^{(i,8)} - c_1^{(i,5)} \,] / 8 \qquad (1d)$$

$$f_{22}^{(i)} = [\, c_2^{(i,3)} - c_2^{(i,2)} + c_2^{(i,4)} - c_2^{(i,1)} + c_2^{(i,7)} - c_2^{(i,6)} + c_2^{(i,8)} - c_2^{(i,5)} \,] / 8 \qquad (1e)$$

$$f_{32}^{(i)} = [\, c_3^{(i,3)} - c_3^{(i,2)} + c_3^{(i,4)} - c_3^{(i,1)} + c_3^{(i,7)} - c_3^{(i,6)} + c_3^{(i,8)} - c_3^{(i,5)} \,] / 8 \qquad (1f)$$

$$f_{13}^{(i)} = [\, c_1^{(i,5)} - c_1^{(i,1)} + c_1^{(i,6)} - c_1^{(i,2)} + c_1^{(i,7)} - c_1^{(i,3)} + c_1^{(i,8)} - c_1^{(i,4)} \,] / 8 \qquad (1g)$$

$$f_{23}^{(i)} = [\, c_2^{(i,5)} - c_2^{(i,1)} + c_2^{(i,6)} - c_2^{(i,2)} + c_2^{(i,7)} - c_2^{(i,3)} + c_2^{(i,8)} - c_2^{(i,4)} \,] / 8 \qquad (1h)$$

$$f_{33}^{(i)} = [\, c_3^{(i,5)} - c_3^{(i,1)} + c_3^{(i,6)} - c_3^{(i,2)} + c_3^{(i,7)} - c_3^{(i,3)} + c_3^{(i,8)} - c_3^{(i,4)} \,] / 8 \qquad (1i)$$

where $c_k^{(i,j)}$ denotes the 'k'th component of the center of mass position vector for nearest neighbor 'j' of particle 'i'. The current (effective) volume for the element is then

$$V^{eff(i)} = 8 \det[\, \underline{\underline{f}}^{(i)} \,] \qquad (2)$$

where 'det' denotes the determinant and the deformation gradient matrix is $\underline{\underline{f}}^{(i)}$.

3. Internal energy

The total internal energy associated with particle 'i' is assumed to consist of particle and element based components, and take the form

$$U = (1/2) \sum_{i=1}^{n} m^{(i)} \, [\, u^{(i)}(v^{(i)}, s^{(i)}) + (1 - D^{(i)}) \, u^{(i)}(\varepsilon^{(i)}, s^{(i)}) \,] \qquad (3a)$$

$$\varepsilon^{(i)} = V^{eff(i)}/m^{(i)} \qquad (3b)$$

where $m^{(i)}$, $u^{(i)}$, $v^{(i)}$, $s^{(i)}$, $D^{(i)}$, and $V^{eff(i)}$ are the mass, internal energy per unit mass, volume per unit mass, entropy per unit mass, continuum damage, and element volume associated with particle 'i'. Since the element volume depends on the particle coordinates $\mathbf{c}(i)$ and since the particle entropy ($S^{(i)}$) and deformation gradient ($F^{(i)}$) are related to the previously defined variables by

$$S^{(i)} = m^{(i)} \, s^{(i)} \quad ; \quad v^{(i)}/v_o^{(i)} = \det(\mathbf{F}^{(i)}) = F^{(i)3} \qquad (3c,d)$$

where $v_o^{(i)}$ is the specific volume in the reference configuration, it follows that the system internal energy can be expressed as a function of the generalized coordinates $\mathbf{c}^{(i)}$, $F^{(i)}$, $D^{(i)}$, and $S^{(i)}$

$$U = U(\mathbf{c}^{(i)}, F^{(i)}, S^{(i)}, D^{(i)}) \qquad (3e)$$

Hence the generalized conservative forces for the system are

$$\mathbf{g}^{eff(i)} = \frac{\partial U}{\partial \mathbf{c}^{(i)}} \qquad (4a)$$

$$G^{(i)} = \frac{\partial U}{\partial F^{(i)}} = - 3 \, V_o^{(i)} \, P^{(i)} \, F^{(i)2} \qquad (4b)$$

$$\theta^{(i)} = \frac{\partial U}{\partial S^{(i)}} = (1/2) \, [\, \theta^{par(i)} + (1 - D^{(i)}) \, \theta^{eff(i)} \,] \qquad (4c)$$

$$\Gamma^{(i)} = - \frac{\partial U}{\partial D^{(i)}} = (1/2) \, m^{(i)} \, u^{(i)}(\varepsilon^{(i)}, s^{(i)}) \qquad (4d)$$

where $\Gamma^{(i)}$ is a damage energy release rate, $P^{(i)}$ is the particle pressure,

$$P^{(i)} = - \frac{\partial u^{(i)}(\nu^{(i)}, s^{(i)})}{\partial \nu^{(i)}} \tag{5a}$$

and the particle and element temperatures are

$$\theta^{par(i)} = \frac{\partial u^{(i)}(\nu^{(i)}, s^{(i)})}{\partial s^{(i)}} \tag{5b}$$

$$\theta^{eff(i)} = \frac{\partial u^{(i)}(\varepsilon^{(i)}, s^{(i)})}{\partial s^{(i)}} \tag{5c}$$

The generalized conservative forces $\mathbf{g}^{eff(i)}$ in equation (4a), associated with the particle center of mass coordinates, may be calculated from the element pressure ($P^{eff(i)}$), which is

$$P^{eff(i)} = - \frac{\partial u^{(i)}(\varepsilon^{(i)}, s^{(i)})}{\partial \varepsilon^{(i)}} \tag{6}$$

and the minor determinants of the element deformation gradient, which are

$$f_{11}^{m(i)} = f_{22}^{(i)} f_{33}^{(i)} - f_{23}^{(i)} f_{32}^{(i)} \tag{7a}$$

$$f_{12}^{m(i)} = f_{31}^{(i)} f_{23}^{(i)} - f_{21}^{(i)} f_{33}^{(i)} \tag{7b}$$

$$f_{13}^{m(i)} = f_{21}^{(i)} f_{32}^{(i)} - f_{31}^{(i)} f_{22}^{(i)} \tag{7c}$$

$$f_{21}^{m(i)} = f_{13}^{(i)} f_{32}^{(i)} - f_{12}^{(i)} f_{33}^{(i)} \tag{7d}$$

$$f_{22}^{m(i)} = f_{11}^{(i)} f_{33}^{(i)} - f_{13}^{(i)} f_{31}^{(i)} \tag{7e}$$

$$f_{23}^{m(i)} = f_{12}^{(i)} f_{31}^{(i)} - f_{11}^{(i)} f_{32}^{(i)} \tag{7f}$$

$$f_{31}^{m(i)} = f_{12}^{(i)} f_{23}^{(i)} - f_{13}^{(i)} f_{22}^{(i)} \quad (7g)$$

$$f_{32}^{m(i)} = f_{13}^{(i)} f_{21}^{(i)} - f_{11}^{(i)} f_{23}^{(i)} \quad (7h)$$

$$f_{33}^{m(i)} = f_{11}^{(i)} f_{22}^{(i)} - f_{12}^{(i)} f_{21}^{(i)} \quad (7i)$$

Equations (6) and (7) then determine the generalized forces for nearest neighbor n1(i) as

$$g_1^{eff(n1(i))} = - (1/2) (1 - D^{(i)}) P^{eff(i)} [- f_{11}^{m(i)} - f_{12}^{m(i)} - f_{13}^{m(i)}] \quad (8a)$$

$$g_2^{eff(n1(i))} = - (1/2) (1 - D^{(i)}) P^{eff(i)} [- f_{21}^{m(i)} - f_{22}^{m(i)} - f_{23}^{m(i)}] \quad (8b)$$

$$g_3^{eff(n1(i))} = - (1/2) (1 - D^{(i)}) P^{eff(i)} [- f_{31}^{m(i)} - f_{32}^{m(i)} - f_{33}^{m(i)}] \quad (8c)$$

The generalized forces for nearest neighbor n2(i) are

$$g_1^{eff(n2(i))} = - (1/2) (1 - D^{(i)}) P^{eff(i)} [f_{11}^{m(i)} - f_{12}^{m(i)} - f_{13}^{m(i)}] \quad (8d)$$

$$g_2^{eff(n2(i))} = - (1/2) (1 - D^{(i)}) P^{eff(i)} [f_{21}^{m(i)} - f_{22}^{m(i)} - f_{23}^{m(i)}] \quad (8e)$$

$$g_3^{eff(n2(i))} = - (1/2) (1 - D^{(i)}) P^{eff(i)} [f_{31}^{m(i)} - f_{32}^{m(i)} - f_{33}^{m(i)}] \quad (8f)$$

The generalized forces for nearest neighbor n3(i) are

$$g_1^{eff(n3(i))} = - (1/2) (1 - D^{(i)}) P^{eff(i)} [f_{11}^{m(i)} + f_{12}^{m(i)} - f_{13}^{m(i)}] \quad (8g)$$

$$g_2^{eff(n3(i))} = - (1/2) (1 - D^{(i)}) P^{eff(i)} [f_{21}^{m(i)} + f_{22}^{m(i)} - f_{23}^{m(i)}] \quad (8h)$$

$$g_3^{eff(n3(i))} = - (1/2) (1 - D^{(i)}) P^{eff(i)} [f_{31}^{m(i)} + f_{32}^{m(i)} - f_{33}^{m(i)}] \quad (8i)$$

The generalized forces for nearest neighbor n4(i) are

$$g_1^{eff(n4(i))} = -(1/2)(1 - D^{(i)})\, P^{eff(i)} [\, -f_{11}^{m(i)} + f_{12}^{m(i)} - f_{13}^{m(i)} \,] \qquad (9a)$$

$$g_2^{eff(n4(i))} = -(1/2)(1 - D^{(i)})\, P^{eff(i)} [\, -f_{21}^{m(i)} + f_{22}^{m(i)} - f_{23}^{m(i)} \,] \qquad (9b)$$

$$g_3^{eff(n4(i))} = -(1/2)(1 - D^{(i)})\, P^{eff(i)} [\, -f_{31}^{m(i)} + f_{32}^{m(i)} - f_{33}^{m(i)} \,] \qquad (9c)$$

The generalized forces for nearest neighbor n5(i) are

$$g_1^{eff(n5(i))} = -(1/2)(1 - D^{(i)})\, P^{eff(i)} [\, -f_{11}^{m(i)} - f_{12}^{m(i)} + f_{13}^{m(i)} \,] \qquad (9d)$$

$$g_2^{eff(n5(i))} = -(1/2)(1 - D^{(i)})\, P^{eff(i)} [\, -f_{21}^{m(i)} - f_{22}^{m(i)} + f_{23}^{m(i)} \,] \qquad (9e)$$

$$g_3^{eff(n5(i))} = -(1/2)(1 - D^{(i)})\, P^{eff(i)} [\, -f_{31}^{m(i)} - f_{32}^{m(i)} + f_{33}^{m(i)} \,] \qquad (9f)$$

The generalized forces for nearest neighbor n6(i) are

$$g_1^{eff(n6(i))} = -(1/2)(1 - D^{(i)})\, P^{eff(i)} [\, f_{11}^{m(i)} - f_{12}^{m(i)} + f_{13}^{m(i)} \,] \qquad (9g)$$

$$g_2^{eff(n6(i))} = -(1/2)(1 - D^{(i)})\, P^{eff(i)} [\, f_{21}^{m(i)} - f_{22}^{m(i)} + f_{23}^{m(i)} \,] \qquad (9h)$$

$$g_3^{eff(n6(i))} = -(1/2)(1 - D^{(i)})\, P^{eff(i)} [\, f_{31}^{m(i)} - f_{32}^{m(i)} + f_{33}^{m(i)} \,] \qquad (9i)$$

The generalized forces for nearest neighbor n7(i) are

$$g_1^{eff(n7(i))} = -(1/2)(1 - D^{(i)})\, P^{eff(i)} [\, f_{11}^{m(i)} + f_{12}^{m(i)} + f_{13}^{m(i)} \,] \qquad (10a)$$

$$g_2^{eff(n7(i))} = - (1/2) (1 - D^{(i)}) P^{eff(i)} [f_{21}^{m(i)} + f_{22}^{m(i)} + f_{23}^{m(i)}] \qquad (10b)$$

$$g_3^{eff(n7(i))} = - (1/2) (1 - D^{(i)}) P^{eff(i)} [f_{31}^{m(i)} + f_{32}^{m(i)} + f_{33}^{m(i)}] \qquad (10c)$$

Finally the generalized forces for nearest neighbor n1(i) are

$$g_1^{eff(n8(i))} = - (1/2) (1 - D^{(i)}) P^{eff(i)} [- f_{11}^{m(i)} + f_{12}^{m(i)} + f_{13}^{m(i)}] \qquad (10d)$$

$$g_2^{eff(n8(i))} = - (1/2) (1 - D^{(i)}) P^{eff(i)} [- f_{21}^{m(i)} + f_{22}^{m(i)} + f_{23}^{m(i)}] \qquad (10e)$$

$$g_3^{eff(n8(i))} = - (1/2) (1 - D^{(i)}) P^{eff(i)} [- f_{31}^{m(i)} + f_{32}^{m(i)} + f_{33}^{m(i)}] \qquad (10f)$$

Note that when the damage for the element associated with particle 'i' is zero, the preceding generalized forces are zero, that is the element looses its cohesion.

4. Plasticity model

Just as the element's nodal displacements determine its current density and hence (in part) its internal energy, the relative velocities of the nodes with respect to the body centered particle determine the local rate of plastic strain. To be specific, the local plastic strain rate at particle 'i' is determined from the tangent relative velocities of particle 'i' with respect to its eight nearest neighbors in the reference configuration

$$\mathbf{v}^{tan(i,j)} = \dot{\mathbf{c}}^{(i)} - \dot{\mathbf{c}}^{(j)} - \mathbf{v}^{rad(i,j)} \quad ; \quad j = 1, 2, \ldots 8 \qquad (11a)$$

where

$$\mathbf{v}^{rad(i,j)} = \{ [(\mathbf{c}^{(i)} - \mathbf{c}^{(j)}) / |\mathbf{c}^{(i)} - \mathbf{c}^{(j)}|] \cdot (\dot{\mathbf{c}}^{(i)} - \dot{\mathbf{c}}^{(j)}) \} [(\mathbf{c}^{(i)} - \mathbf{c}^{(j)}) / |\mathbf{c}^{(i)} - \mathbf{c}^{(j)}|] \qquad (11b)$$

Given a yield stress ($\sigma^{y(i)}$) and current volume ($V^{(i)}$) for the particle, the force on particle 'i' associated with plastic flow is

$$f_k^{p(i)} = \sum_{j=1}^{8} f^{p(i,j)} \; \text{sign}[\, v_k^{\tan(i,j)} \,] \qquad (11c)$$

where

$$f^{p(i,j)} = [\, 1 / (h^{(i)} + h^{(j)})] \, [\, 1 - \min(D^{(i)}, D^{(j)}) \,] \, (1/2) \, (\, V^{(i)} \, \sigma^{y(i)} + V^{(j)} \, \sigma^{y(j)} \,) \qquad (11d)$$

The effective plastic strain ($\varepsilon^{p(i)}$) is then calculated by integrating the rate equation

$$\dot{\varepsilon}^{p(i)} = (2/3) \sum_{j=1}^{8} \{ \, [\, 1 / (h^{(i)} + h^{(j)})] \, | \, \mathbf{v}^{\tan(i,j)} \, | \, \}^2 \qquad (11e)$$

for each particle.

5. Damage evolution

The damage evolution relation assumed here is the simplest possible, namely the damage is set to one when the plastic strain in an element reaches a user specified critical value. This value is normally termed an erosion or failure strain in the finite element literature. The introduction of more complex damage evolution relations and other failure criteria is relatively simple, and is under consideration for future versions of the analysis code.

6. Entropy production

The effects of plastic deformation and damage evolution must be accounted for in the entropy evolution relations, since plastic flow and damage evolution are dissipative processes. An irreversible entropy production rate for particle 'i' ($\dot{S}^{irr(i)}$) is calculated from the energy dissipation rate associated with plastic deformation and damage evolution, as follows:

$$\dot{S}^{irr(i)} = (1 / \theta^{(i)}) \, [\, \mathbf{f}^{p(i)} \cdot \dot{\mathbf{c}}^{(i)} + \Gamma^{(i)} \, \dot{D}^{(i)} \,] \qquad (12)$$

The coefficients of the generalized velocities in the entropy production relations will determine nonconservative generalized forces in the system level state equations.

7. Example simulations

Appendices A, B, and C, show some example hypervelocity impact simulations performed using the code EXOS.

The first example represents the oblique impact of a spherical projectile on a flat plate at 6.81 kilometers per second. Both the projectile and the shield were taken to be aluminum, with the material described by a Mie-Grüneisen equation of state. Parameters of the simulation are shown in Appendix A. Figures A-1, A-2, and A-3 show the simulation results.

The second example represents the oblique impact of a cylindrical projectile on a flat plate at 7.0 kilometers per second. Again both the projectile and plate materials were taken to be aluminum, and a Mie-Grüneisen equation of state was used. Parameters of the simulation are shown in Appendix B. Figures B-1, B-2, B-3, and B-4 show the simulation results.

The third example represents the oblique impact of a rod on a flat plate at 7.0 kilometers per second. Again both the projectile and plate materials were taken to be aluminum, and a Mie-Grüneisen equation of state was used. Parameters of the simulation are shown in Appendix C. Figures C-1, C-2, C-3, and C-4 show the simulation results.

8. Conclusion

This report details the formulation and implementation of a finite element augmentation for the particle hydrodynamics model of Fahrenthold and Koo (1997). The coupling of particle based and finite element based models in a single code allows for the general characterization of both contact-impact effects and elastic-plastic-damage effects, important to the simulation of hypervelocity impacts on space structures.

References

Fahrenthold, E.P., and Koo, J.C., "Hamiltonian Particle Hydrodynamics," *Computer Methods in Applied Mechanics and Engineering*, Vol. 146 (1997), pp. 43-52.

Hallquist, J.O., 1983, Theoretical Manual for DYNA3D, Lawrence Livermore National Laboratory.

APPENDIX A: Sphere impact simulation

Simulation parameters; oblique impact of a sphere on a flat plate:

Sphere diameter (aluminum)	=	1.00 cm
Impact velocity	=	6.81 cm/μsec
Impact obliquity	=	15 degrees
Plate thickness (aluminum)	=	0.16 cm
Equation of state type	=	Mie-Grüneisen
Failure strain	=	0.50
Yield stress	=	0.0029 Mbar
Numerical shear viscosity coefficient	=	0.01
Numerical bulk viscosity coefficient	=	0.10
Numerical conduction coefficient	=	1.00
Penalty stiffness coefficient	=	10.0
Time step coefficient	=	10.0
Number of particles	=	17,530
Total simulation time	=	3.00 μsec
Number of time steps	=	3,210
CPU time (Cray J916)	=	2.82 hours

List of figures (attached):

Figure A-1. Oblique view: simulation a t = 0.0 μsec.

Figure A-2. Oblique view: simulation a t = 3.0 μsec.

Figure A-3. Normal view: simulation a t = 3.0 μsec.

Figure A-1

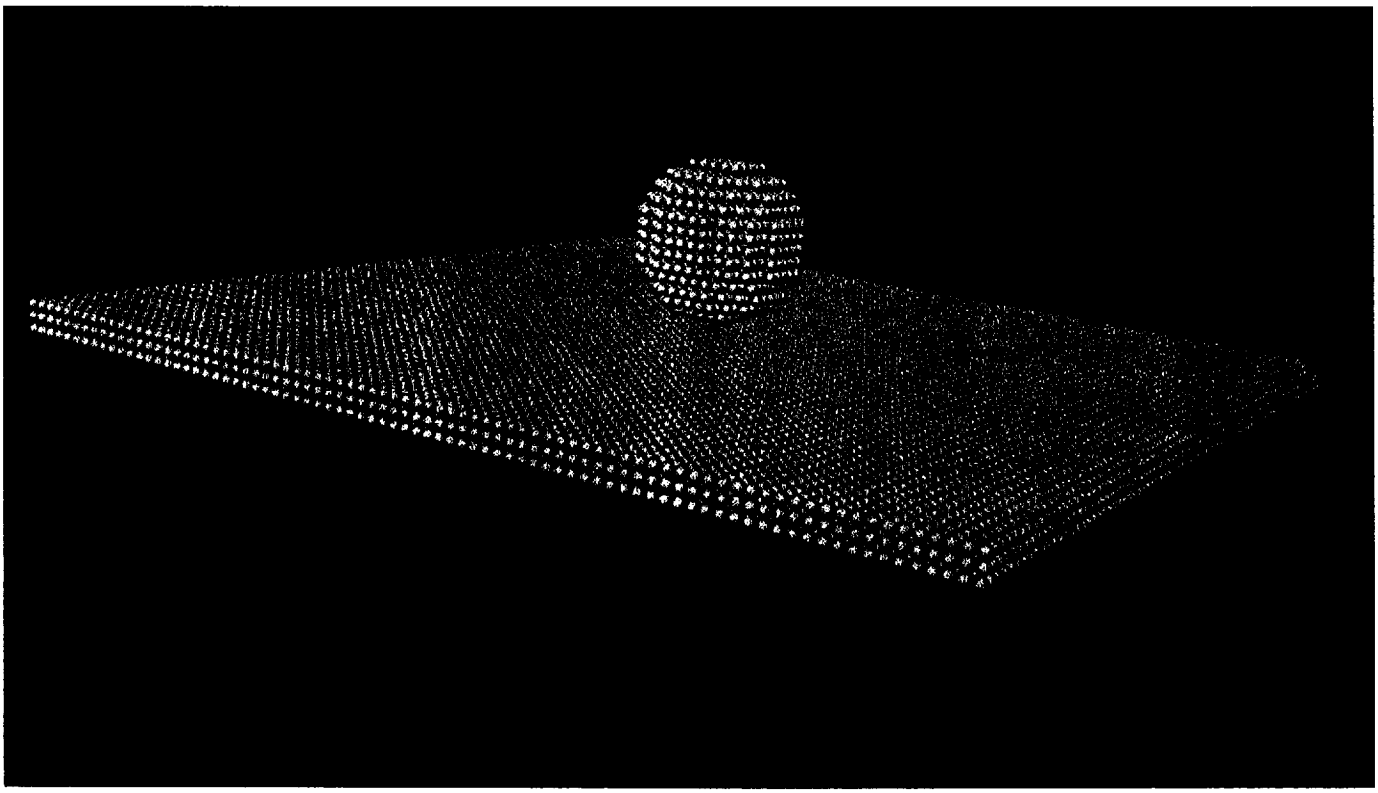

Figure A-2

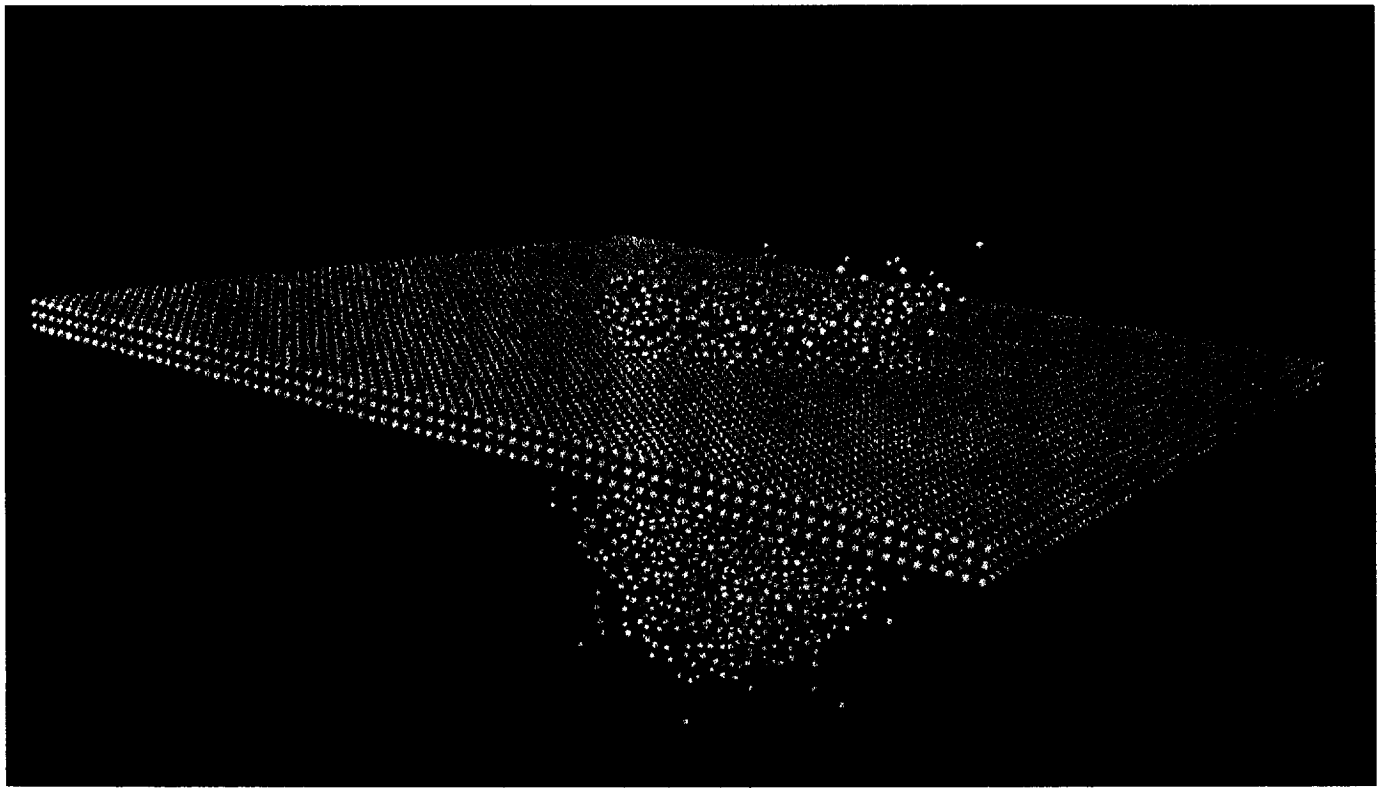

Figure A-3

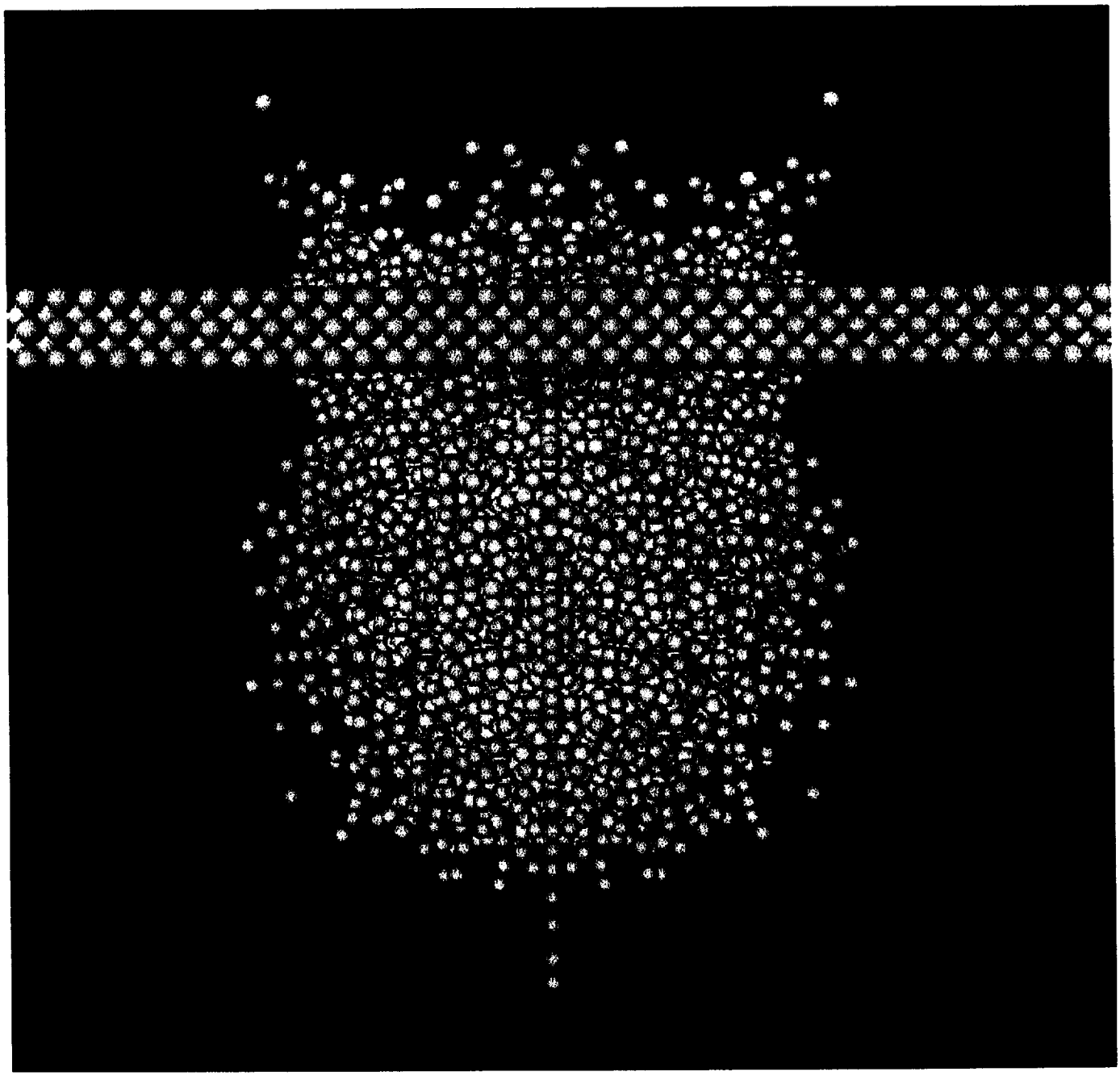

APPENDIX B: Cylinder impact simulation

Simulation parameters; oblique impact of a cylinder on a flat plate:

Cylinder diameter (aluminum)	=	0.20 cm
Cylinder length	=	0.40 cm
Impact velocity	=	7.00 cm/μsec
Impact obliquity	=	31 degrees
Plate thickness (aluminum)	=	0.04 cm
Equation of state type	=	Mie-Grüneisen
Failure strain	=	0.50
Yield stress	=	0.0029 Mbar
Numerical shear viscosity coefficient	=	0.01
Numerical bulk viscosity coefficient	=	0.10
Numerical conduction coefficient	=	1.00
Penalty stiffness coefficient	=	10.0
Time step coefficient	=	10.0
Number of particles	=	11,184
Total simulation time	=	2.00 μsec
Number of time steps	=	7,772
CPU time (Cray J916)	=	4.66 hours

List of figures (attached):

Figure B-1. Oblique view: simulation a t = 0.00 μsec.

Figure B-2. Oblique view: simulation a t = 1.21 μsec.

Figure B-3. Oblique view: simulation a t = 2.00 μsec.

Figure B-4. Normal view: simulation a t = 2.00 μsec.

Figure B-1

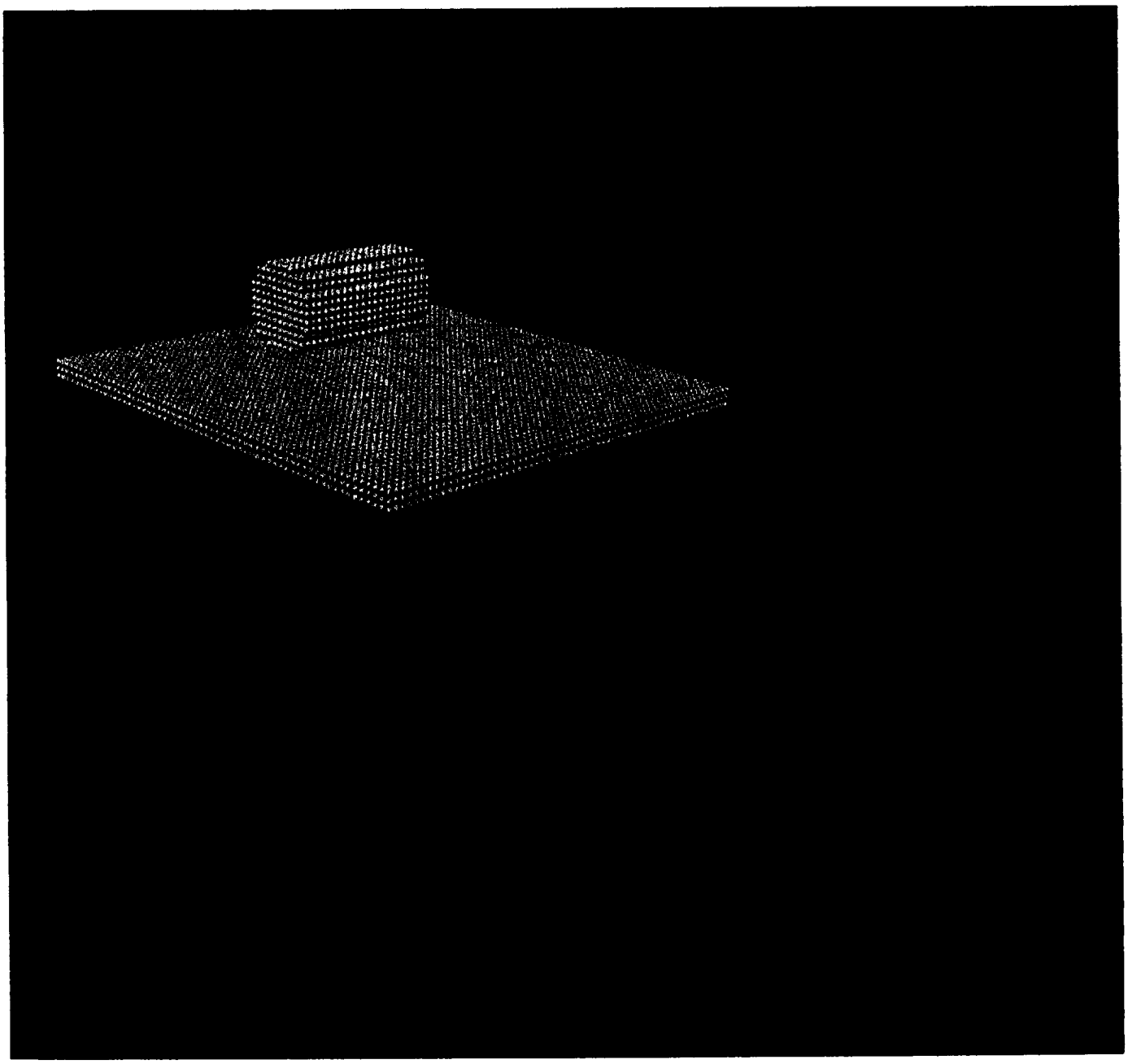

Figure B-2

Figure B-3

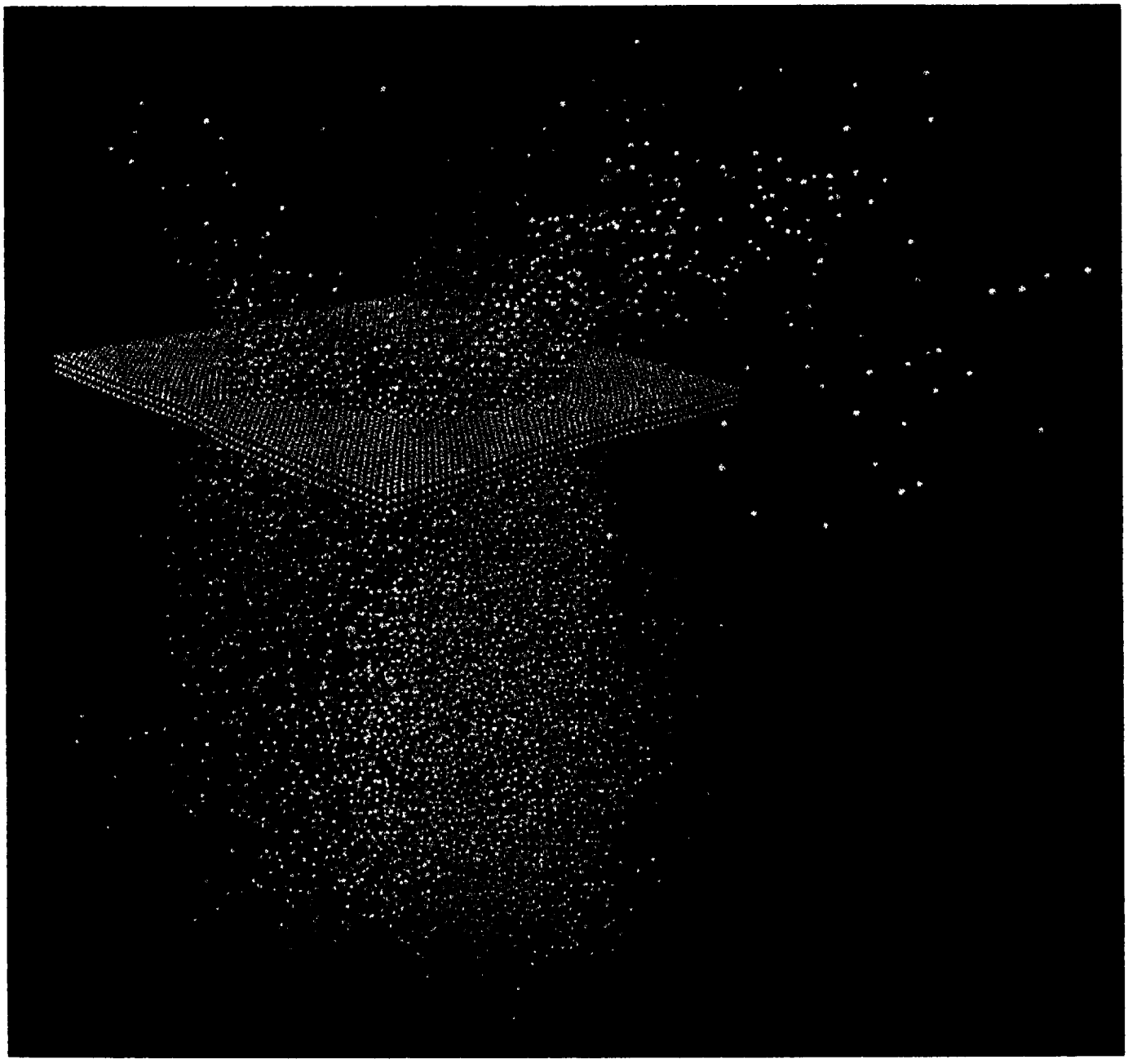

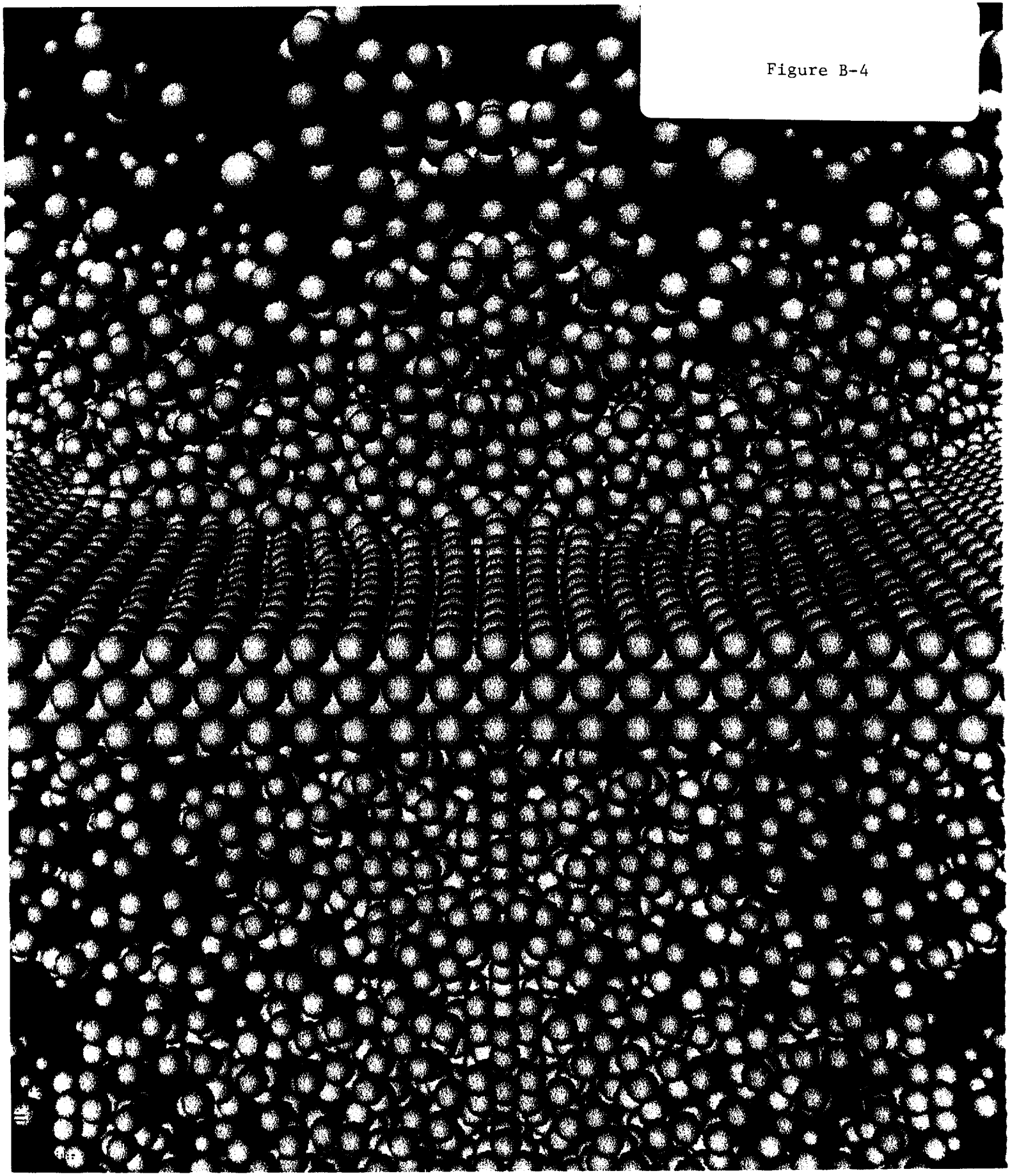

Figure B-4

APPENDIX C: Rod impact simulation

Simulation parameters; oblique impact of a rod on a flat plate:

Cylinder diameter (aluminum)	=	0.08 cm
Cylinder length	=	0.24
Impact velocity	=	7.00 cm/μsec
Impact obliquity	=	31 degrees
Plate thickness (aluminum)	=	0.04 cm
Equation of state type	=	Mie-Grüneisen
Failure strain	=	0.50
Yield stress	=	0.0029 Mbar
Numerical shear viscosity coefficient	=	0.01
Numerical bulk viscosity coefficient	=	0.10
Numerical conduction coefficient	=	1.00
Penalty stiffness coefficient	=	10.0
Time step coefficient	=	10.0
Number of particles	=	23,754
Total simulation time	=	1.00 μsec
Number of time steps	=	7,959
CPU time (Cray J916)	=	8.04 hours

List of figures (attached):

Figure C-1. Oblique view: simulation a t = 0.000 μsec.

Figure C-2. Oblique view: simulation a t = 0.206 μsec.

Figure C-3. Oblique view: simulation a t = 0.627 μsec.

Figure C-4. Oblique view: simulation a t = 1.000 μsec.

Figure C-1

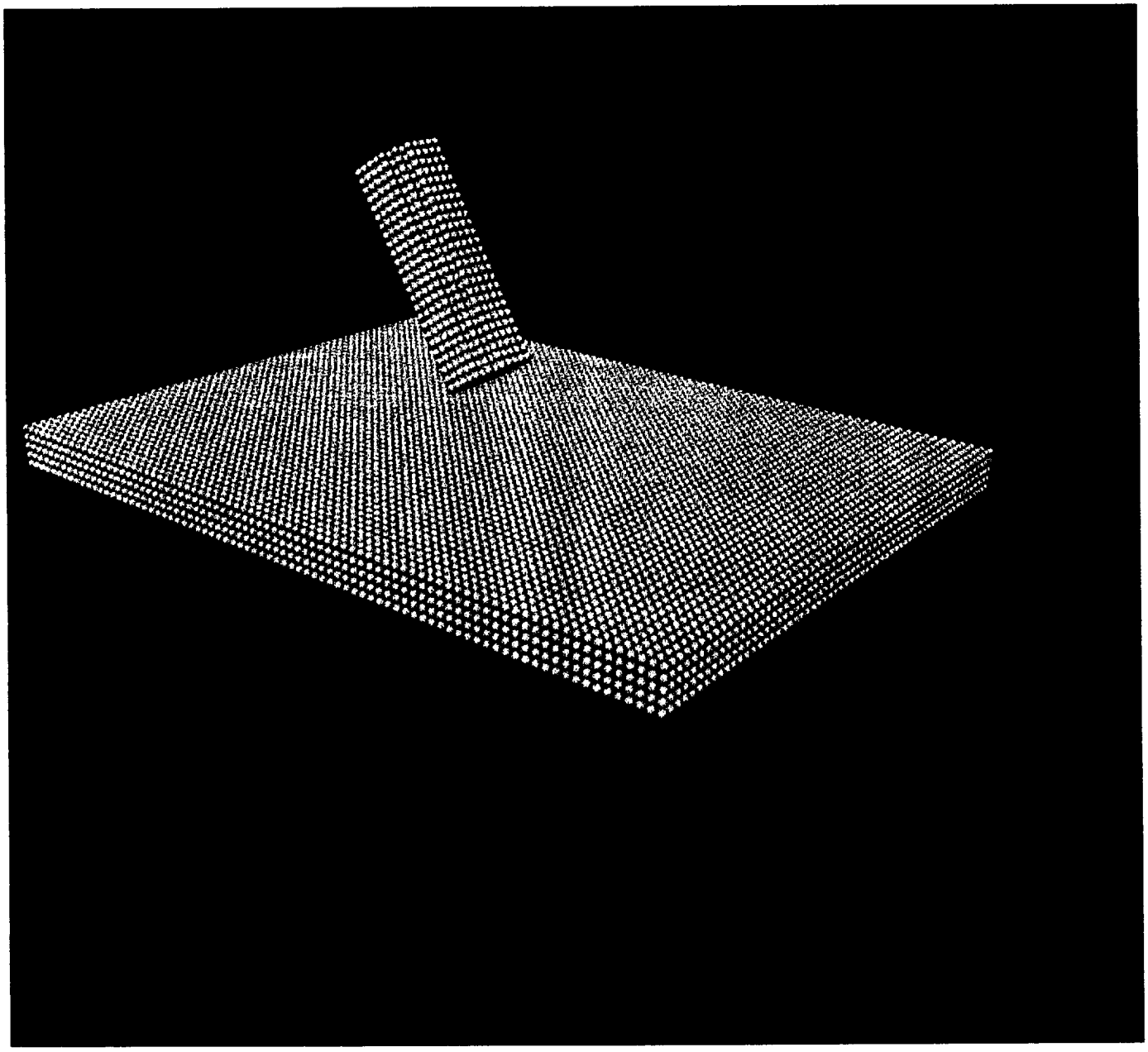

Figure C-2

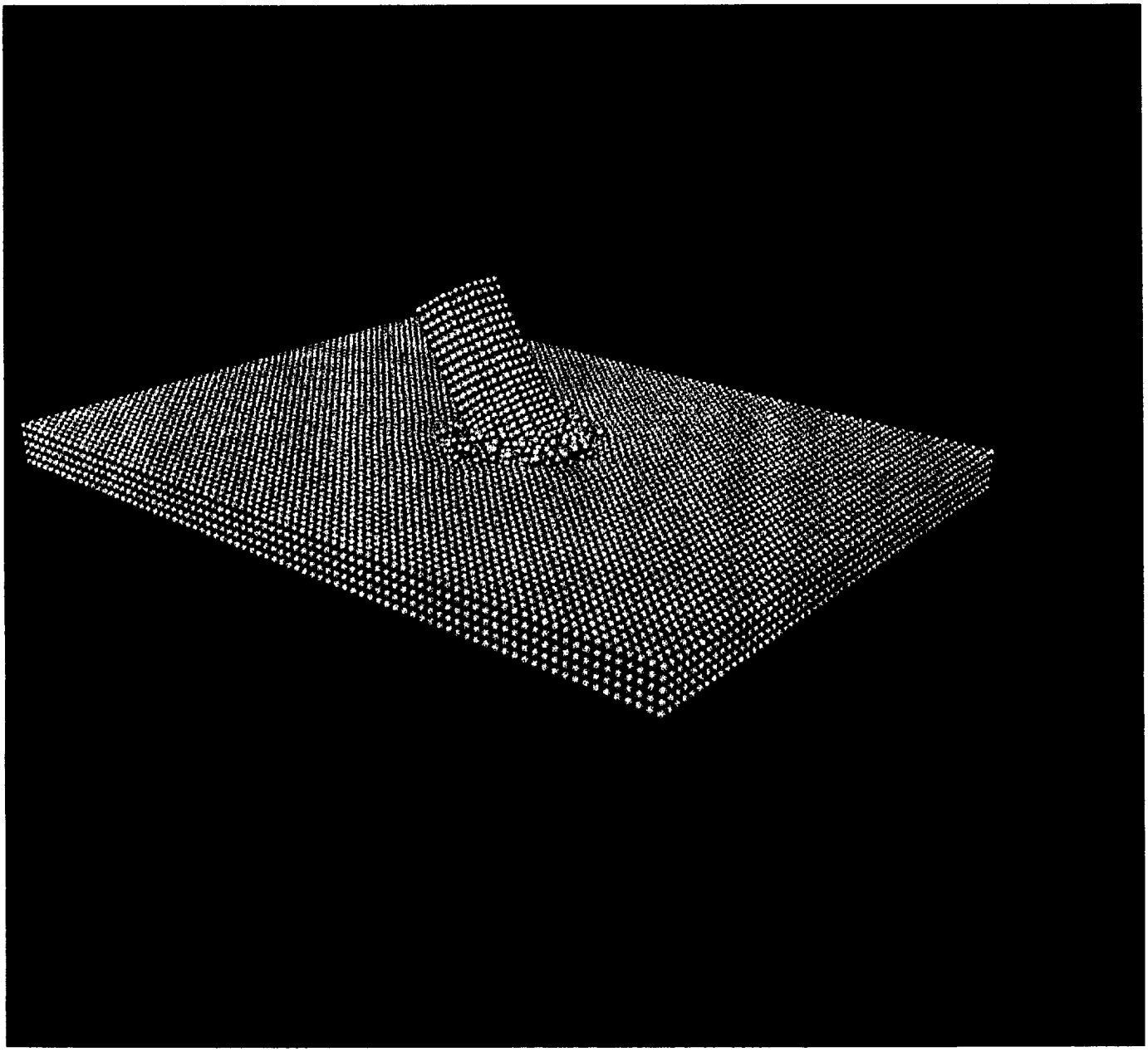

Figure C-3

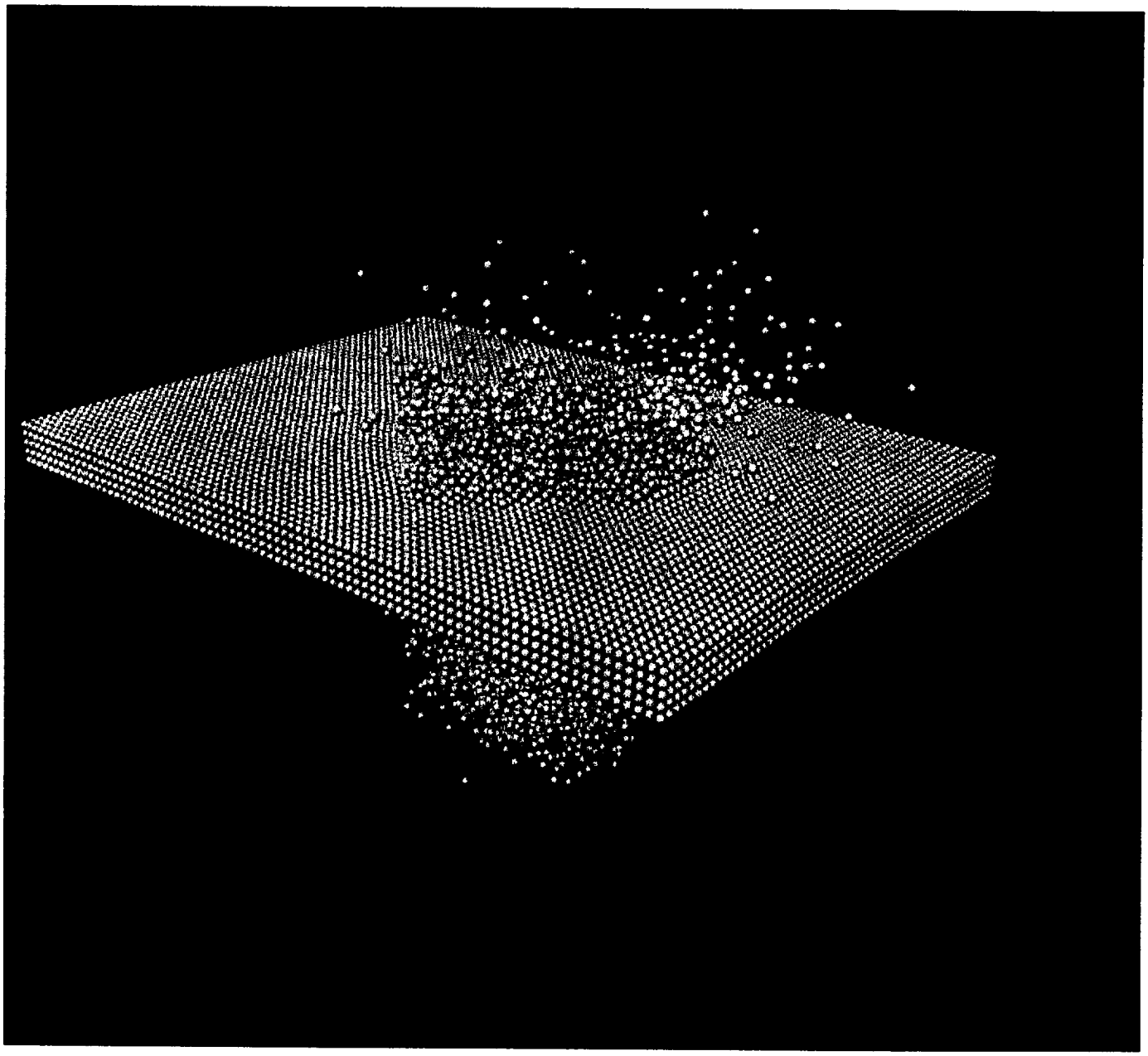

Figure C-4